Author/s:
Jiao, J;He, Y;Kentish, SE;Ashokkumar, M;Manasseh, R;Lee, J

Title:
Experimental and theoretical analysis of secondary Bjerknes forces between two bubbles in a standing wave

Date:
2015-04-01

Citation:
Jiao, J., He, Y., Kentish, S. E., Ashokkumar, M., Manasseh, R. & Lee, J. (2015). Experimental and theoretical analysis of secondary Bjerknes forces between two bubbles in a standing wave. Ultrasonics, 58, pp.35-42. https://doi.org/10.1016/j.ultras.2014.11.016.

Persistent Link:
https://hdl.handle.net/11343/55180

Experimental and theoretical analysis of secondary Bjerknes forces between two bubbles in a standing wave

Junjie Jiao[1, 2], Yong He[1]*, Sandra E. Kentish[3], Muthupandian Ashokkumar[2],
Richard Manasseh[4] and Judy Lee[3]*

[1]Department of Mechanical Engineering, Nanjing University of Science and Technology, Jiangsu, China
[2]Particulate Fluids Processing Centre, School of Chemistry, University of Melbourne, Parkville, VIC. 3010 Australia; Adjunct Professor, Chemistry Department, King Abdulaziz University, Jeddah, Saudi Arabia.
[3]Particulate Fluids Processing Centre, Chemical and Biomolecular Engineering, University of Melbourne, Parkville, VIC, 3010 Australia
[4]Mechanical Engineering, Faculty of Engineering & Industrial Sciences, Swinburne University of Technology, Hawthorn, VIC, 3122, Australia

Corresponding Authors: jytlee@unimelb.edu.au; yhe1964@mail.njust.edu.cn

Key words: secondary Bjerknes force; frequency; pressure; bubble size; approach velocity; acceleration

ABSTRACT

Bubbles in an acoustic field are affected by forces such as primary and secondary Bjerknes forces, which have been shown to be influenced by acoustic pressure, frequency, bubble size and separation distance between bubbles. However, such studies are predominantly theoretical, and are mostly focused on the sign reversal of the secondary Bjerknes force. This study provides experimental data on the effect of a range of bubble sizes (8 - 30 μm), distances (≤ 0.2 mm), acoustic pressures (20 - 40 kPa) and frequencies (40 – 100 kHz) on the relative acceleration of two approaching bubbles. Under these conditions, only variations in the magnitude of the attractive force were observed. Using coupled equations of radial and translational motions, the acceleration and secondary Bjerknes force were calculated and compared to the experimental data. The variations in the magnitude of the secondary Bjerknes forces were explained by simulating bubble radius and coupled volume oscillation as a function of time.

1. INTRODUCTION

The secondary Bjerknes force is a time-averaged interaction force between two bubbles driven in an acoustic field, named after C. A. Bjerknes and his son V. F. K Bjerknes[1]. These authors derived a theoretical expression for this force with the following assumptions: (i) The surrounding medium is incompressible; (ii) the gas behaves adiabatically; (iii) the bubble size is smaller than their distance of separation and the bubbles remain spherical; (iv) any higher order scattering from the bubbles is negligible compare to the primary scattering and (v) the driving pressure is low and the bubbles oscillate linearly with the driving frequency. Under these conditions, the secondary Bjerknes force is repulsive if the driving frequency lies between the resonance frequencies of the two bubbles, otherwise the force is attractive[2]. This has been verified experimentally by Kuznetsov[3] and Crum[4]. However, this linear theory fails to describe experimental observations of stable bubble clusters, which can only be explained by a reversal in the secondary Bjkernes force from attractive to repulsive. Oguz and Prosperetti[5] were able to theoretically demonstrate the sign reversal in the secondary Bjerknes force by considering nonlinear bubble oscillations at high driving pressures. However, their analysis was only applicable for bubbles that are far apart.

When the distance of separation is comparable to the bubble size or when the driving pressure is high, assumptions (i), (iii) and (iv) are no longer valid. Zabolotskaya[6, 7] modified Bjerknes' classical linear theory to account for twofold scattered waves from bubbles, this was later extended by Doinikov and Zavtrak[8] to consider multiple scattering between the bubbles. Both concluded that when bubbles, driven below resonance, move closer to each other, the natural frequency of the multibubble system shifts. This phase shift in the bubble oscillation can change the sign of the secondary Bjerknes force. A similar result was reported by Ida[9-11], and by Pelekasis and Tsamopoulos[12, 13] who allowed for shape deviations of the bubbles from sphericity, caused by subharmonic resonances. Doinikov[14] derived an expression to allow for translational oscillations of the bubbles, the vorticity of the linear scattered field and acoustic streaming, and demonstrated that viscous effects can cause repulsion between bubbles driven below resonance. Barbat et al.[15, 16] modified the linear theory for the secondary Bjerknes force by introducing a model for the coupling between the pulsations of the bubbles' interfaces. This model allowed a more general evaluation of the dynamic behavior of bubble motion.

Although there are many theoretical studies in the literature, these are mainly focused on the conditions which cause the sign change in the secondary Bjerknes force and are often reported in a set of contour plots[14, 17, 18] showing regions of attraction and repulsion in a range of bubble radii, driving frequencies and pressures. There are in fact small variations in the magnitude of the secondary Bjerknes force within the regions of attraction and repulsion that are rarely discussed. Experimental evidence of the secondary Bjerknes force is limited due to the practical difficulties in measuring these forces in an acoustic field[8], especially at short separation distances where the secondary Bjerknes force is the main dominant force[19]. Therefore, existing experimental studies are either qualitative[20, 21] or restricted to long bubble-bubble separations (> 2 mm) and large bubble sizes in the order of millimeters[4, 16]. Recently, trajectory and sign change in secondary Bjerknes force for bubbles with sizes in the micrometer range and with shorter distances have been reported[17, 22, 23], however, these experiments were conducted with the bubbles near or adhered to a surface. In addition, due to difficulties associated with these experiments, usually one ultrasound frequency and power level alone is studied.

In this study, the trajectories of two micrometer size bubbles, trapped in an acoustic standing wave field, were measured experimentally to obtain the relative acceleration and secondary Bjerknes force. Different acoustic frequencies, powers, bubble sizes and separations were investigated. The experimental data were compared against theoretical predictions of secondary Bjerknes forces using coupled equations of radial and translational motions reported by Doinikov[24] and explained via a different visualisation of the simulation. The results will be of interest for understanding and modeling bubble dynamics in an acoustic field.

2. EXPERIMENTAL AND THEORETICAL DETAILS

2.1 EXPERIMENTAL DETAILS

An imaging system (Figure 1 (a)), similar to that described by Jiao et al.[19], was used to collect experimental data. A cylindrical Pyrex cell containing two parallel flat surfaces for viewing and back lighting purposes was used. A hollow cylindrical transducer was attached to the bottom of the cell. The transducer (Z7, American Piezo Ceramics Inc., Mackeyville, PA, U.S.A.) was driven at the required frequency (20 kHz – 100 kHz) by a frequency generator (HM8131-2, Hameg Instruments GmBH, Mainhausen, Germany) coupled to a power amplifier (Model 7500, Krohn-Hite, Avon, MA, U.S.A.). The bubble images were magnified using a long-distance microscope, and recorded using a high-speed video camera (Y4-PIV, IDT, Tallahassee, FL, U.S.A.) at a rate of 2000 frames per second. The acoustic pressure was measured using an interchangeable 1 mm PVdF needle hydrophone (Precision Acoustics Ltd, Dorchester, Dorset, U.K.). The hydrophone also allowed the antinode to be accurately located. The acoustic pressures used in this study ranged from 20 ± 1 kPa to 40 ± 1 kPa.

For bubble generation, water was first degassed to avoid any cavitation that could affect the translational motion of the two approaching bubbles. Using a syringe needle, one bubble was first injected and trapped at the pressure antinode, followed by the injection of a second bubble. The trajectory of the two approaching bubbles were recorded and analyzed frame by frame using ImageJ[25] to determine the bubble position, velocity and acceleration as a function of time. An example of the images captured as a function of time is shown in Figure 1(b). The error associated with the determination the bubble size is approximately ± 2.6 μm. It was difficult to control the size of the bubbles injected. Therefore, Table 1 lists the range of bubble sizes investigated. Although these were single run experiments, we verified the reproducibility of the data for a given system (data provided in the supplementary information). The translational movement of bubbles in an acoustic field is controlled by the acoustic and hydrodynamic forces. Note that the secondary Bjerknes force is significantly higher than the primary Bjerknes force when bubbles are close to each other (at distances ≤ 0.2 mm)[19]. Hence, the focus of this study was the translational motion of bubbles when the distance between two bubbles was less or equal to 0.2 mm.

2.2 MATHEMATICAL MODEL

The relative acceleration and secondary Bjerknes force theoretically predicted was calculated using a previously published simulation model involving coupled equations of radial and translational motions. Details on the model can be found in other references[18, 19, 26]. The model is briefly discussed below.

The pressure gradient in an acoustic field can cause a bubble to move, thus experiencing a changed pressure. These changes can influence the bubble's oscillation, which in turn can affect the bubble's translational motion. Therefore, both bubble translation and oscillation mutually influence each other when the bubbles move in an acoustic field. Doinikov[26, 27] used the Lagrangian formalism to obtain two coupled ordinary differential equations of second order for radial pulsation (Eq. 1) and translational motions (Eq. 2) of a gas bubble along the *y* axis:

$$R\ddot{R} + \frac{3}{2}\dot{R}^2 - \frac{P_{sc}}{\rho} = \frac{\dot{y}^2}{4} \qquad (1)$$

$$\ddot{y} + \frac{3\dot{R}\dot{y}}{R} = \frac{3F_{ey}}{2\pi\rho R^3} \qquad (2)$$

where R is the time-dependent radius, ρ is the liquid density and F_{ey} denotes the external forces on the bubble such as the primary Bjerknes force and the viscous drag*.

---

* It is worth noting that contrary to the commonly used drag force of $-12\pi\mu R\dot{x}$ where $\dot{x}$ is the bubble velocity and μ is the liquid viscosity, a much lower drag force of $-4\pi\mu R\dot{x}$ was used in the simulation by assuming the additional history force (F_{bb}) is negligible: $F_{bb} = 8\pi\mu\int_0^t exp\left(\frac{9\upsilon s}{R^2}\right) erfc\left[\sqrt{\frac{9\upsilon s}{R^2}}\right] R\ddot{x}(s)ds$. This equation can be simplified to: $F_{bb} = 8\pi\mu\int_0^t exp\left(-\frac{1}{3}\frac{9\upsilon s}{R^2}\right) R\ddot{x}(s)ds$, where υ is the kinematic viscosity, and F_{bb} was found by inserting a typical experimental value, an approximate F_{bb} was found to be two orders of magnitude lower than the drag force.

The time-varying bubble radius can be calculated based on the Keller-Miksis equation [28]. However, in a two-bubble environment, the Keller-Miksis equation needs to be expanded to include the influence of the neighboring bubble. If the bubble shapes are assumed to remain spherical for all times with radii R_1 and R_2, the respective pressure generated by bubble 2 on bubble 1, and vice versa, is given by Eq.3[18]:

$$P = \frac{\rho}{r_{12}}(R_2\ddot{R}_2 + 2\dot{R}_2^{\,2}) \qquad (3)$$

where r_{12} is the separation distance between the two bubbles. By incorporating Eq. 3 into the Keller-Miksis equation, the oscillation of bubble 1 was obtained:

$$\left(1-\frac{\dot{\mathrm{R}}_1}{\mathrm{c}}\right)R_1\ddot{R}_1 + \frac{3}{2}\dot{R}_1^{\,2}\left(1-\frac{\dot{R}_1}{3c}\right) = \frac{\dot{y}^2}{4} + \left(1+\frac{\dot{\mathrm{R}}_1}{\mathrm{c}}\right)\frac{p_{sc}}{\rho} + \frac{R}{\rho c}p_{sc} - \frac{\rho}{r_{12}}(R_2\ddot{R}_2 + 2\dot{R}_2^{\,2}) \qquad (4)$$

$$p_{sc} = \left(p_0 + \frac{2\sigma}{R_{10}}\right)\left(\frac{R_{10}}{R_1}\right)^{3\kappa} - p_0 - \frac{2\sigma}{R_1} - \frac{4\mu}{R_1}\dot{R}_1 - P_{ex} \qquad (5)$$

where R_{10} is the equilibrium radius of bubble 1, p_0 is the hydrostatic pressure, σ is the surface tension, κ is the polytropic exponent of the gas within the bubble and P_{ex} is the external driving signal that is defined for the standing wave as in Eq. 6:

$$P_{ex} = P_a \sin(\omega t)\cos(k r_{12}) \qquad (6)$$

where ω is the angular frequency and k is the wave number. Exchanging indices 1↔2, we get the equations for bubble 2.

The secondary Bjerknes force (F_B) is calculated using Eq.7:

$$F_B = \frac{\rho}{4\pi r_{12}^2}\langle \dot{V}_1 \dot{V}_2 \rangle = \frac{4\pi\rho}{r_{12}^2}\langle R_1^2 \dot{R}_1 R_2^2 \dot{R}_2 \rangle \quad (7)$$

where V_1 and V_2 are the respective volumes of bubble 1 and bubble 2. Eq. 7 shows that the volume change in one acoustic cycle is related to both the change in radii of the two bubbles (R_1 and R_2) and their radial velocities ($\dot{R}_1$ and $\dot{R}_2$).

The physical parameters used in this study, unless otherwise indicated, are: ρ = 998 kg/m^3, P_0 = 101.3 kPa, c = 1480 m/s, σ = 0.072 N/m, γ = 1.4 and μ = 0.001 Pa/s.

3. RESULTS AND DISCUSSION

The trajectories of two approaching bubbles were captured under different frequencies and pressures. Selected trajectories of bubbles with similar sizes, driven under the same acoustic pressure but different frequencies, are shown in Figure 2. For all frequencies, the approach velocity increases as the distance between the two bubbles is reduced. Although 80 kHz and 100 kHz appear to have similar approach velocities, they are much faster compare to the two lower frequencies. This can be explained by the higher frequencies being much closer to the linear resonance frequency of the bubbles and thus gives rise to a greater attractive secondary Bjerknes force. However, for 60 kHz, which is closer to the linear resonance frequency of the bubbles than 40 kHz, the approach velocity appears to be slower compared to 40 kHz. Even though we aimed to select bubbles of similar sizes, R_1 for 60 kHz is a lot smaller than R_2 compared to other frequencies. As the difference in the bubble sizes becomes larger, the oscillation of the two bubbles becomes increasingly out of phase and consequently decreases the attractive secondary Bjerknes force between the two bubbles. Due to the difficulties associated with controlling the size of the bubbles, the data collected consists of a range of bubble size pairs. Therefore, to better present the experimental data, the relative acceleration for a given pair of bubbles is mapped out in R_1-R_2 space for two different acoustic pressures (see Figure 3). This acceleration is indicated by the numbers adjacent to each of the experimental data points. The value was determined from the trajectory of the approaching bubbles at a separation of 0.2 mm. The variations in the size of bubbles, as well as the magnitude of the relative acceleration, are apparent in this figure. In general, the relative acceleration appears to increase for a larger pair of bubbles; this is clearly observed for 100 kHz. For unequal size bubble pairs, the variation in the relative acceleration is more complex.

To validate and understand these experimentally observed variations, a contour map of the secondary Bjerknes force, theoretically predicted using Eq. 7, is also mapped out in Figure 3 against the experimental data. Under the experimental conditions studied, the predicted secondary Bjerknes force is all attractive, with its magnitude denoted by the intensity of the shading. For a given frequency and power, the relative changes in the experimental acceleration aligns well with the variations observed in the theoretically predicted secondary Bjerknes force. That is, the acceleration and magnitude of this force both increase as the size of bubbles becomes larger.

The comparison between experimental and theoretically predicted acceleration is presented in Figure 4. The Figure includes the data shown in Figure 3 as well as additional data for acoustic pressures of 20 kPa obtained at a bubble separation of 0.15 mm. The experimental data, which are all independent measurements, show good agreement with the theoretically predicted values despite some scattering in the data. However, more importantly, the data scatter is uniform –

there is no indication of a bias towards lower or higher values. This suggests that the theoretical model used is correct and it is experimental variability that creates the scatter.

Although the effect of bubble sizes on the secondary Bjerknes force has been studied before[18, 29, 30], the existing reports are theoretical studies predicting the changes in the sign of the secondary Bjerknes force for bubble driven close to resonance. Although the secondary Bjerknes forces shown in Figure 3 are all attractive, there exits significant variations in the magnitude of the secondary Bjerknes force as a function of the two bubble sizes. For equal sized bubbles, it is apparent that the magnitude of the attractive force increases as a function of the bubble size, but the variation in the secondary Bjerknes force for unequal size bubbles is less obvious. To illustrate this, the variation in the secondary Bjerknes force along the horizontal line, shown in Figure 5 (a) - (c), is plotted as a function of increasing bubble 1 radius for four different acoustic pressures. For 40 kHz and 80 kHz (Figure 5 (d) and (e)), the secondary Bjerknes force passes through a series of maxima and minima as the size of bubble 1 increases. Whereas, for 100 kHz a gradual increase in the secondary Bjerknes force is observed (Figure 5 (f)). In general, for a given bubble size pair, increasing acoustic pressure raises the magnitude of the secondary Bjerknes force, except for 80 kHz where the secondary Bjerknes force remains unaffected by pressure at the bubble size of 11 µm and 14 µm.

Modeling of the bubble dynamics was undertaken to explain the fluctuations in the secondary Bjerknes force observed in Figure 5. It is known that the secondary Bjerknes force is related to the average volume oscillation of two bubbles (Eq. 7). Therefore, the fluctuations in $\langle \dot{V}_1 \dot{V}_2 \rangle$ for one acoustic cycle for 80 kHz and 40 kPa, shown in Figure 5 (e), are plotted as a function of increasing bubble 1 size in Figure 6. As Bubble 1 increases in size from 9 µm to 10 µm, the average of $\langle \dot{V}_1 \dot{V}_2 \rangle$ becomes more positive and the secondary Bjerknes force increases. However a further increase in the bubble size from 10 μm to 11 μm results in a decrease in the secondary Bjerknes force owing to the average in $\langle \dot{V}_1 \dot{V}_2 \rangle$ becoming less positive. This is more pronounced as the size of bubble 1 shifts from 11 μm to 17 μm with the average $\langle \dot{V}_1 \dot{V}_2 \rangle$ passing through a maximum at approximately 14 μm. No repulsion was observed in the frequency, power and bubble size investigated.

The effect of increasing acoustic pressure on $\langle \dot{V}_1 \dot{V}_2 \rangle$ is shown in Figure 7 for bubble pairs corresponding to the minimum (unequal size bubbles with radii of 11 μm and 14 μm) and maximum (equal size bubbles with 14 μm radius) points in Figure 5e. For unequal size pairs where bubbles would be oscillating out of phase to each other, increasing acoustic pressure enhanced the amplitude of $\langle \dot{V}_1 \dot{V}_2 \rangle$ in both the positive and negative directions which resulted in very little change in the secondary Bjerknes force. Conversely, for equal size bubbles oscillating in-phase, increasing acoustic pressure enhanced the amplitude of the $\langle \dot{V}_1 \dot{V}_2 \rangle$ in the positive sense, resulting in an average increase in the secondary Bjerknes force as observed in Figure 5e.

The effect of the distance between bubbles on the secondary Bjerknes force is demonstrated in Figure 8, where the bubble radius and $\langle \dot{V}_1 \dot{V}_2 \rangle$ time curves for 11 μm and 14 μm radius bubbles, driven at 80 kHz and 40 kPa, are simulated at three different separations. The linear resonance frequencies of 11 μm and 14 μm radius bubbles are 317 kHz and 246 kHz, respectively. Therefore, the driving frequency is close to ¼ subharmonic of the 11 μm bubble and $^1/_3$ subharmonics of the 14 μm bubble. This is reflected in the higher order harmonics observed from the bubble radius time curves. For bubble 2, the higher harmonics disappears as it moves closer to bubble 1. The variation in the oscillation of bubble 2 causes the oscillation of the two bubbles to be more in-phase as the bubbles becomes closer. This is manifested in the amplitude of $\langle \dot{V}_1 \dot{V}_2 \rangle$, which is more positive when the two bubbles are oscillating in phase (this is observed for *t/T* between 0 - 0.2) and becomes more negative with time when the oscillations becomes out of phase. For these two bubbles, as they become closer, the bubble oscillations around *t/T* = 0.8 becomes more in phase, giving an enhanced $\langle \dot{V}_1 \dot{V}_2 \rangle$ in the positive direction, which will translate to a stronger attractive force.

4. CONCLUSIONS

In this study, we have experimentally obtained the trajectories and relative accelerations between two approaching bubbles under a range of acoustic frequencies, pressures, bubble sizes and separations. Under these conditions, the secondary Bjerknes forces were all attractive and only variations in the magnitude of the forces were observed. Using a previously published simulation model involving coupled equations of radial and translational motions, we have demonstrated that the observed variations were caused by differences in the size of bubbles, which was shown to affect the magnitude of the coupled volume oscillations and hence the magnitude of the secondary Bjerknes force.

ACKNOWLEDGEMENTS

We are grateful to Prof Yos Morsi for facilitating the use of the high-speed camera and for detailed comments on a draft of this paper. The financial support through the Australian

Research Council for the DECRA (Discovery Early Career Research Award, DE120101567) is also gratefully acknowledged.

REFERENCES

[1]V. Bjerknes, Fields of force. The Columbia University Press: New York, 1906.
[2]A. A. Doinikov, "Effects of the second harmonic on the secondary Bjerknes force," Phys. Rev. E, ***59***, 3016 (1999)
[3]G. N. Kazantsev, "Motion of bubbles in a liquid under the action of Bjerknes forces arising in an acoustic field," Sov. Phys. Dokl., ***4***, 1250 (1960)
[4]L. A. Crum, "Bjerknes forces on bubbles in a stationary sound field," J. Acoust. Soc. Am, ***57***, 1363 (1975)
[5]H. N. Oguz and A. Prosperetti, "A generalization of the impulse and virial theorems with an application to bubble oscillations," J. Fluid Mech, ***218***, 143 (1990)
[6]E. A. Zabolotskaya, " Phase conjugation of sound beams in connection with four-phonon interaction in a liquid containing gas bubbles," Sov. Phys. Acoust, ***30***, 365 (1984)
[7]E. A. Zabolotskaya, "Nonlinear waves in liquid with gas bubbles," Tr. Inst. Ob. Fiz. Akad. Nauk, ***18***, 121 (1989)
[8]A. A. Doinikov and S. T. Zavtrak, "On the mutual interaction of two gas bubbles in a sound field," Phys. Fluids ***7***, 1923 (1995)
[9]M. Ida, "A characteristic frequency of two mutually interacting gas bubbles in an acoustic field," Phys. Lett. A, ***297***, 210 (2002)
[10]M. Ida, "Number of transition frequencies of a system containing an arbitrary number of gas bubbles," J. Phys. Soc. Jpn, ***71***, 1214 (2002)
[11]M. Ida, "Alternative interpretation of the sign reversal of secondary Bjerknes force acting between two pulsating gas bubbles," Phys. Rev. E, ***67***, 056617 (2003)
[12]N. A. Pelekasis and J. A. Tsamopoulos, "Bjerknes forces between two bubbles. Part 1. Response to a step change in pressure," J. Fluid Mech, ***254***, 467 (1993)
[13]N. A. Pelekasis and J. A. Tsamopoulos, "Bjerknes forces between two bubbles. Part 2. Response to an oscillatory pressure field," J. Fluid Mech, ***254***, 501 (1993)
[14]A. A. Doinikov, "Viscous effects on the interaction force between two small gas bubbles in a weak acoustic field," J. Acoust. Soc. Am, ***111***, 1602 (2002)
[15]T. Barbat and N. Ashgriz, "Planar dynamics of two interacting bubbles in an acoustic field," Appl. Math. Comput, ***157***, 775 (2004)
[16]T. Barbat, N. Ashgriz and L. Chingshi, "Dynamics of two interacting bubbles in an acoustic field," J. Fluid Mech, ***389***, 137 (1999)
[17]K. Yoshida, T. Fujikawa and Y. Watanabe, "Experimental investigation on reversal of secondary Bjerknes force between two bubbles in ultrasonic standing wave," J. Acoust. Soc. Am, ***130***, 135 (2011)
[18]R. Mettin, I. Akhatov, U. Parlitz, C. D. Ohl and W. Lauterborn, "Bjerknes forces between small cavitation bubbles in a strong acoustic field," Phys. Rev. E ***56***, 2924 (1997)
[19]J. Jiao, Y. He, T. Leong, S. E. Kentish, M. Ashokkumar, R. Manasseh and J. Lee, "Experimental and theoretical studies on the movements of two bubbles in an acoustic standing wave field," J. Phys. Chem. B, ***117***, 12549 (2013)

[20]M. Kornfeld and L. Suvorov, "On the destructive action of cavitation," Journal of Applied Physics, ***15***, (1944)
[21]F. Blake Jr, "Bjerknes forces in stationary sound fields," The Journal of the Acoustical Society of America, ***21***, (1949)
[22]X. Xi, F. Cegla, R. Mettin, F. Holsteyns and A. Lippert, "Collective bubble dynamics near a surface in a weak acoustic standing wave field," J. Acoust. Soc. Am, ***132***, 37 (2012)
[23]X. Xi, F. B. Cegla, M. Lowe, A. Thiemann, T. Nowak, R. Mettin, F. Holsteyns and A. Lippert, "Study on the bubble transport mechanism in an acoustic standing wave field," Ultrasonics, ***51***, 1014 (2011)
[24]A. A. Doinikov, "Translational motion of two interacting bubbles in a strong acoustic field," Phy. Rev. E, ***64***, 026301-1 (2001)
[25]W. S. Rasband, ImageJ, U. S. National Institutes of Health, Bethesda, Maryland, USA, http://imagej.nih.gov/ij/, 1997-2014. ,
[26]A. A. Doinikov, "Translational motion of a spherical bubble in an acoustic standing wave of high intensity " Phys. Fluids A, ***14***, 1420 (2002)
[27]A. A. Doinikov, "Translational motion of a spherical bubble in an acoustic standing wave of high intensity," Phys. Fluids, ***14***, 1420 (2002)
[28]J. B. Keller and M. Miksis, "Bubble oscillations of large amplitude," J. Acoust. Soc. Am., ***68***, 628 (1980)
[29]N. A. Pelekasis, A. Gaki, A. Doinikov and J. A. Tsamopoulos, "Secondary Bjerknes forces between two bubbles and the phenomenon of acoustic streamers," Journal of Fluid Mechanics, ***500***, (2004)
[30]A. Harkin, T. JKaper and A. Nadim, "Coupled pulsation and translation of two gas bubbles in a liquid," J. Fluid Mech, ***445***, 377 (2001)

TABLE 1: For pressures ranging from 20 to 40 kPa, a range of bubble sizes were captured under four different frequencies.

	Bubble 1 [μm]	Bubble 2 [μm]
40 kHz	8 - 24	12 - 27
60 kHz	5.5 - 21	6.5 - 24
80 kHz	11 - 20	11 - 19.5
100 kHz	8 - 17	6.5 - 16

Figure 1:(a) Imaging system for observing the trajectory of two approaching bubbles in an acoustic standing wave field and (b) selected images illustrating the movement of two attracting bubbles driven at a frequency of 22.4 kHz and 50 kPa.

Figure 2: Centre positions of two approaching bubbles as a function of time under different frequencies driven at an acoustic pressure of 30 kPa. The radius of bubble 1, R_1 (top trajectory), and bubble 2, R_2 (bottom trajectory), are shown in the legend as [R_1, R_2].

Figure 3: Map of the magnitude of the secondary Bjerknes force (in N) determined from Equation 7 for different frequencies and acoustic pressures. The experimentally measured relative acceleration between two approaching bubbles of a given size is also plotted. The number next to the data denotes the magnitude of the acceleration in m/s^2. For both simulated and experimental data, values were calculated or obtained at a bubble distance of 0.2 mm, taken from the centre of the bubble.

Figure 4: Comparison between the simulated and experimental relative acceleration for two approaching bubbles of various radii and pressures at different acoustic frequencies. In each graph, the solid line indicates when the experimental and simulated data match (x=y). For both simulated and experimental data, values were calculated or obtained at a bubble distance of 0.15 and 0.2 mm, taken from the centre of the bubble.

Figure 5: Secondary Bjerknes force for different frequencies: (a) and (d) 40 kHz, (b) and (e) 80 kHz, and (c) and (f) 100 kHz at an acoustic pressure of 40 kPa. (a) - (c) maps out the secondary Bjerknes force for various pairs of bubble sizes and (e) - (f) graphs the variation in the secondary Bjerknes force along the solid line depicted in (a) - (c) for different pressures. The distance between the bubbles is fixed at 0.2 mm.

Figure 6: Bubble coupled volume as a function of increasing bubble 1 size (radius in micrometers is denoted on the right) while bubble 2 is fixed at 14 µm. The frequency is 80 kHz and the acoustic pressure 40 kPa (*t* is the time and *T* is the time of one acoustic cycle). $\langle \dot{V}_1 \dot{V}_2 \rangle$ = 0 is indicated by the dotted line.

Figure 7: Bubble coupled volume change with increasing acoustic pressure for the bubble pair corresponding to the minimum (left-hand column) and maximum (right-hand column) points in Figure 5e (*t* is the time and *T* is the time of one acoustic cycle; bubble 2 is fixed at 14 µm).

Figure 8: Bubble radius and coupled volume change at 80 kHz and 40 kPa when the distance between bubbles are: (a) 0.2 mm (b) 0.1 mm (c) 0.05mm. (*t* is the time and *T* is the time of one acoustic cycle; the initial radii are 14 µm and 11 µm, for bubble 1 and 2, respectively).

Figure 1a

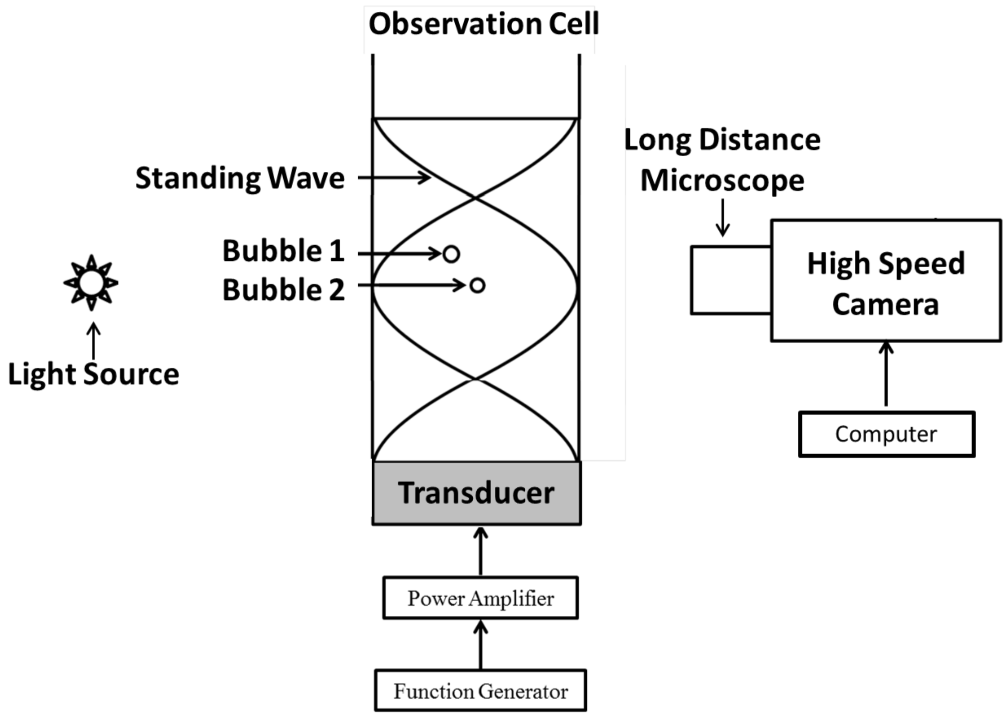

Figure 1b

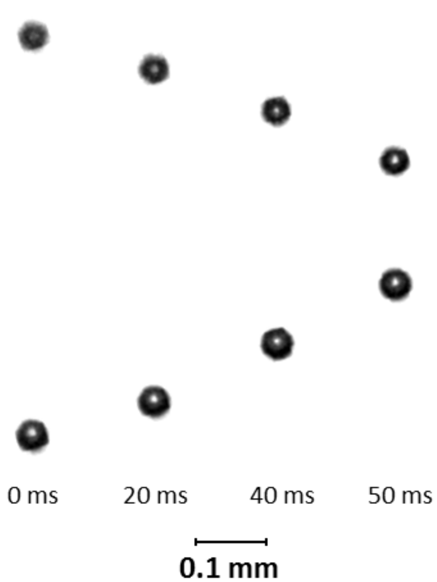

Figure 2

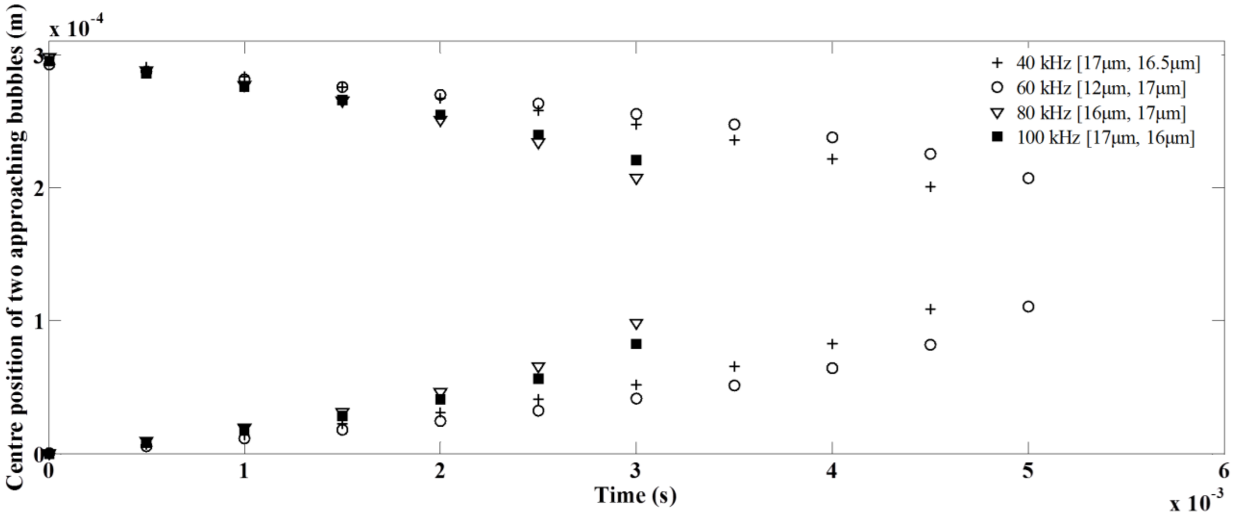
x 10^-4
Centre position of two approaching bubbles (m)
Time (s)
x 10^-3
+ 40 kHz [17µm, 16.5µm]
○ 60 kHz [12µm, 17µm]
▽ 80 kHz [16µm, 17µm]
■ 100 kHz [17µm, 16µm]
0
1
2
3
4
5
6

Figure 3

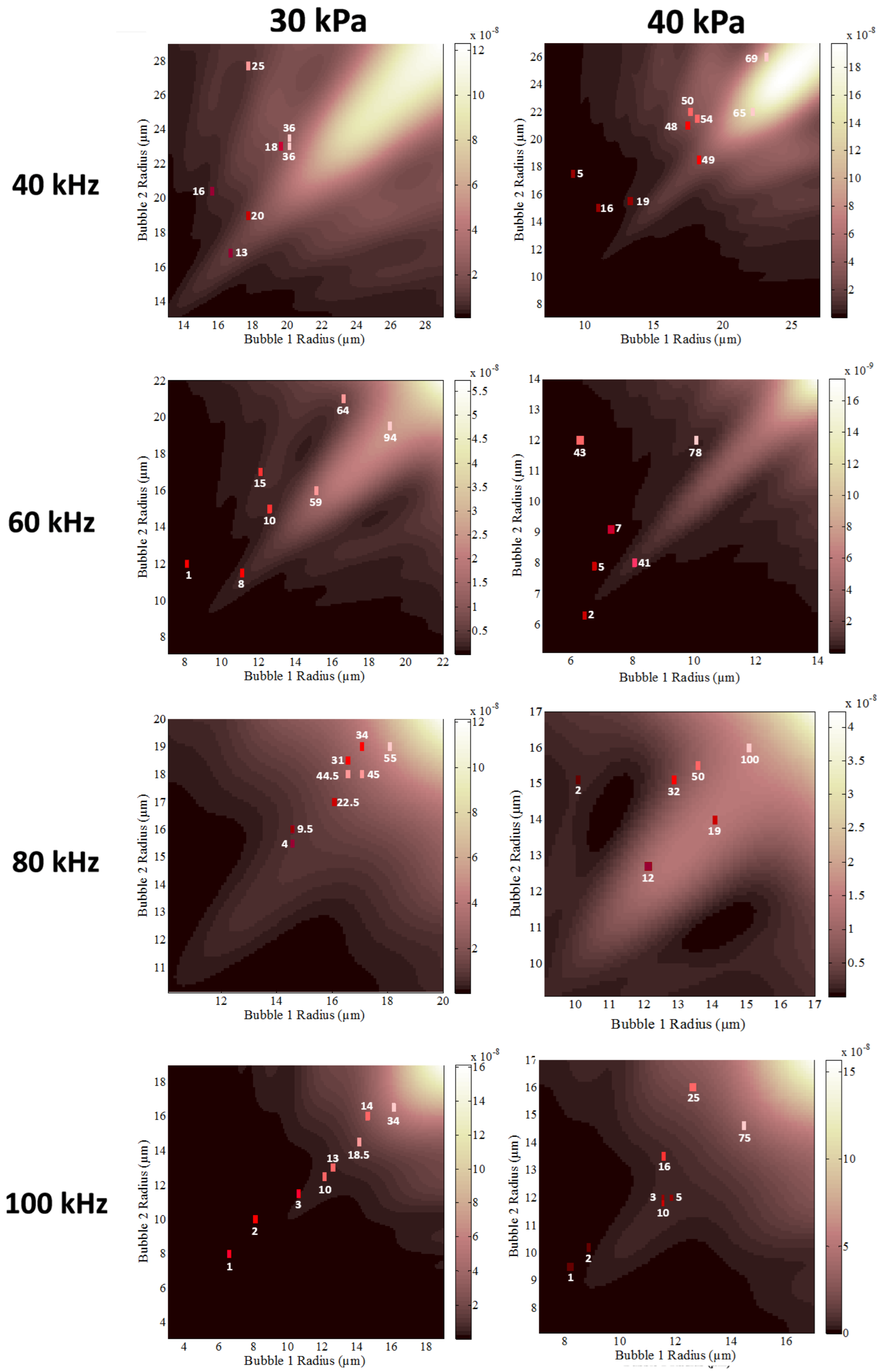

30 kPa
40 kPa
40 kHz
60 kHz
80 kHz
100 kHz
Bubble 1 Radius (µm)
Bubble 2 Radius (µm)

Figure 4

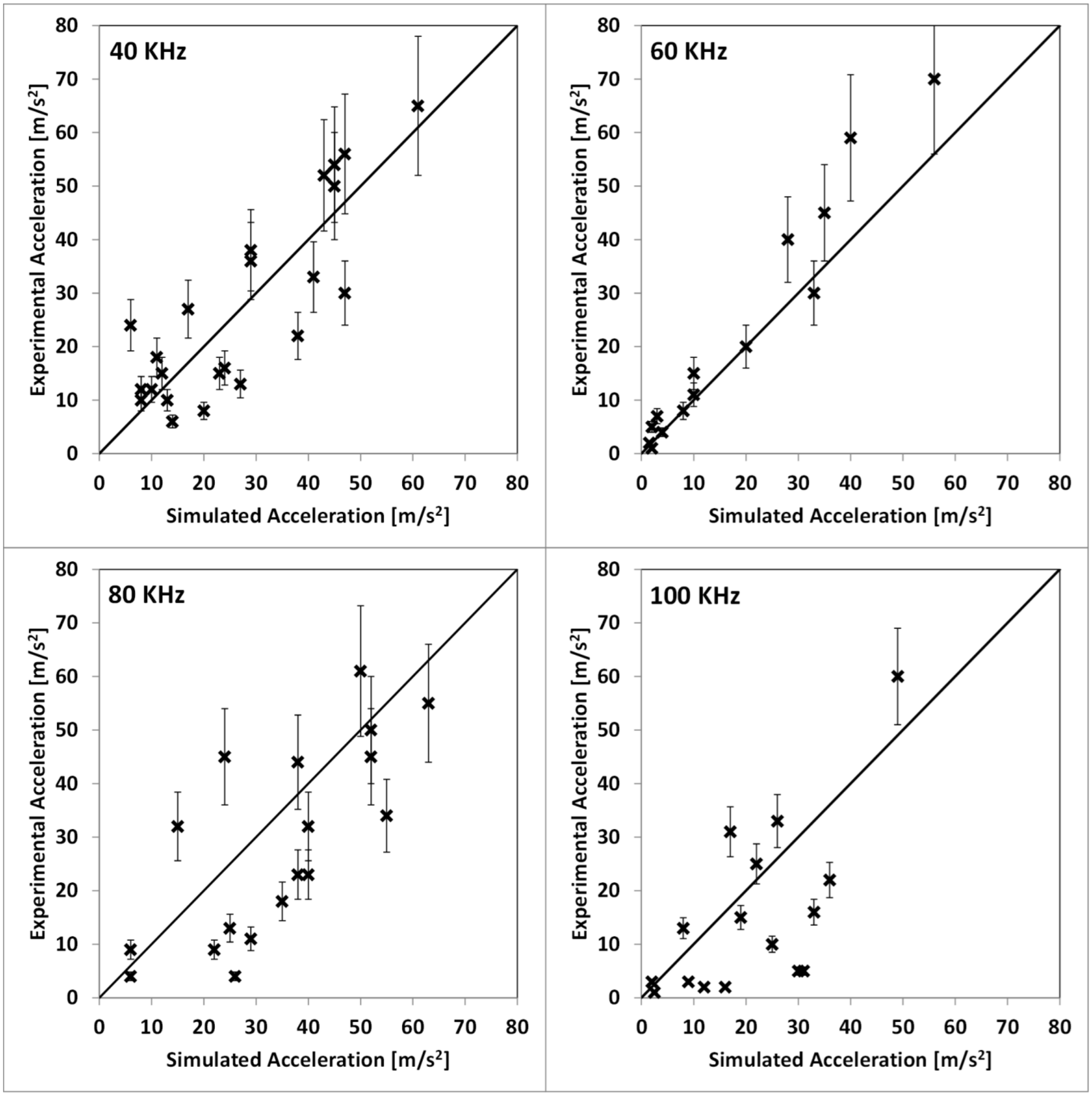
40 KHz
60 KHz
80 KHz
100 KHz
Experimental Acceleration [m/s²]
Simulated Acceleration [m/s²]
0
10
20
30
40
50
60
70
80

Figure 5

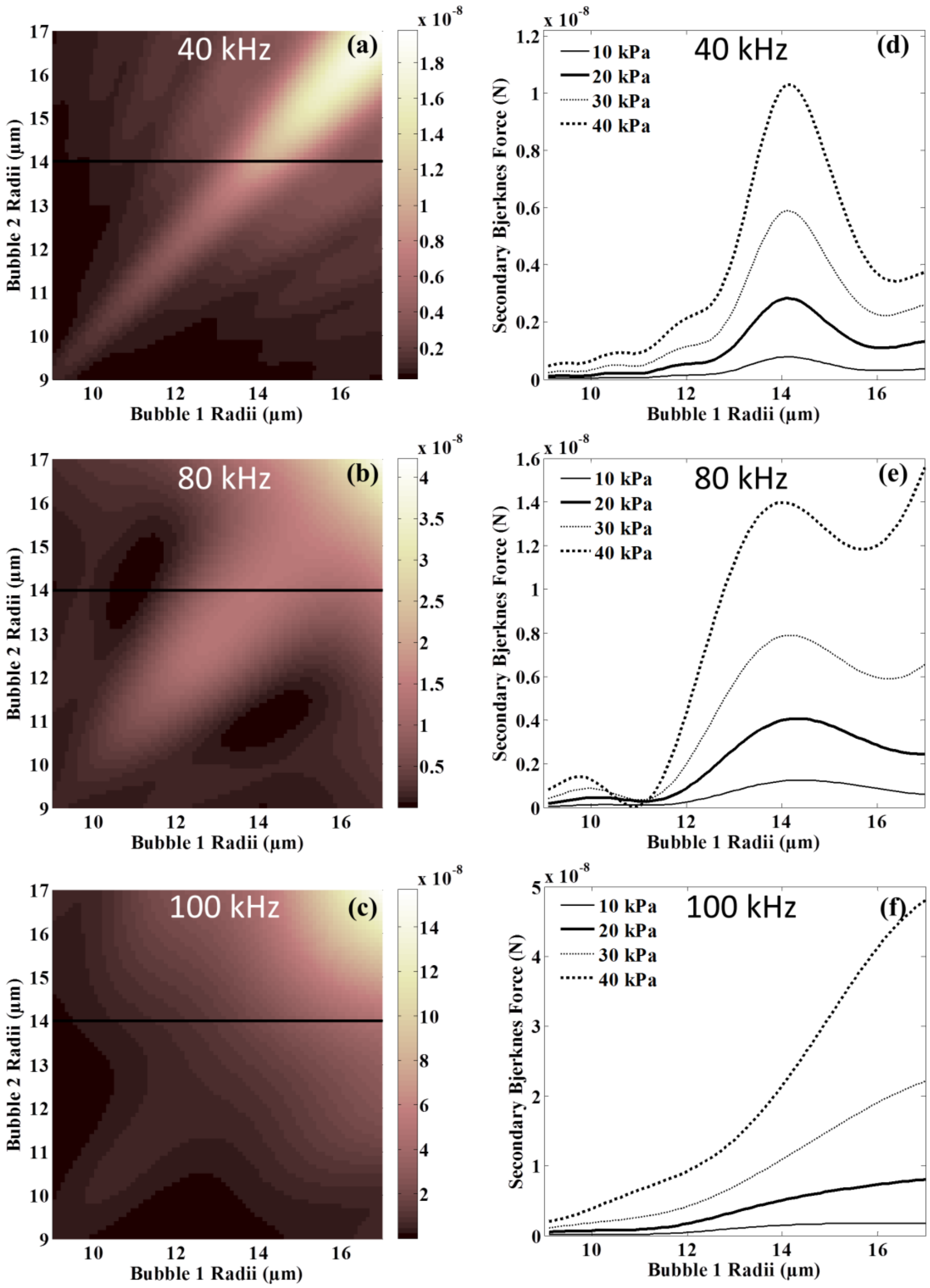
40 kHz
(a)
Bubble 2 Radii (µm)
Bubble 1 Radii (µm)
x 10^-8
80 kHz
(b)
100 kHz
(c)
Secondary Bjerknes Force (N)
10 kPa
20 kPa
30 kPa
40 kPa
(d)
(e)
(f)

Figure 6

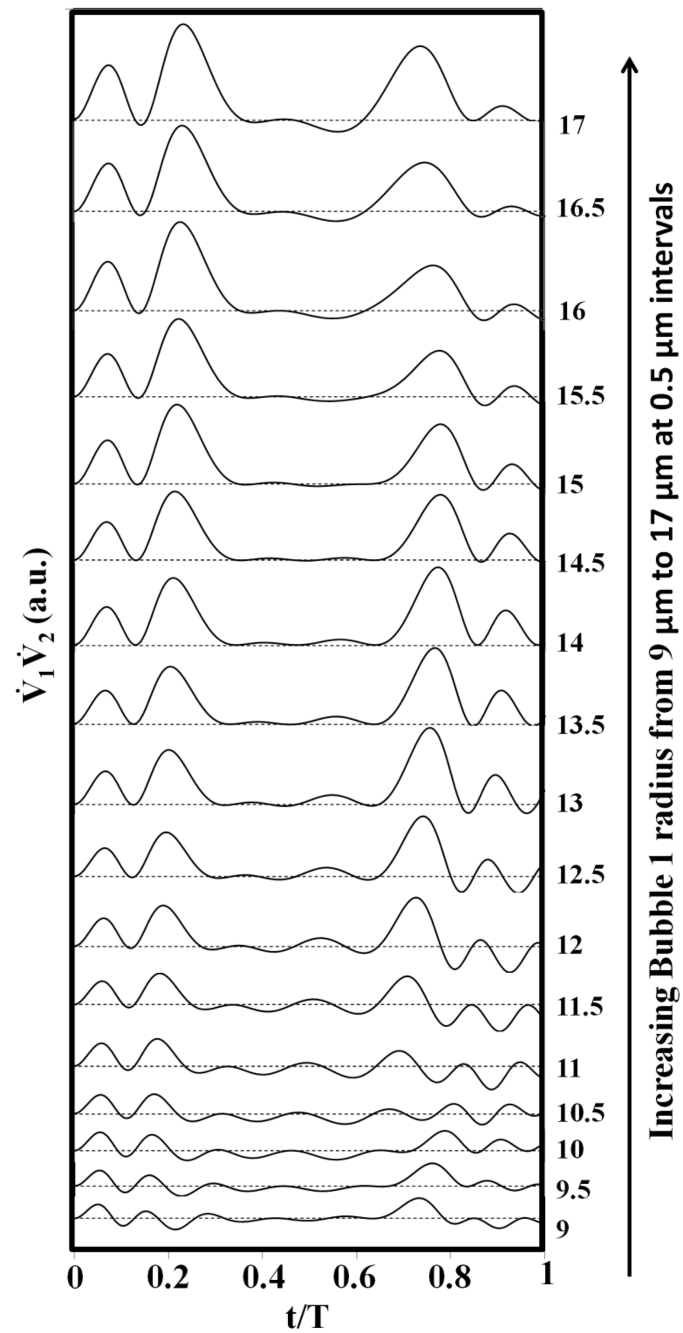

$\dot{V}_1\dot{V}_2$ (a.u.)
17
16.5
16
15.5
15
14.5
14
13.5
13
12.5
12
11.5
11
10.5
10
9.5
9
0
0.2
0.4
0.6
0.8
1
t/T
Increasing Bubble 1 radius from 9 μm to 17 μm at 0.5 μm intervals

Figure 7

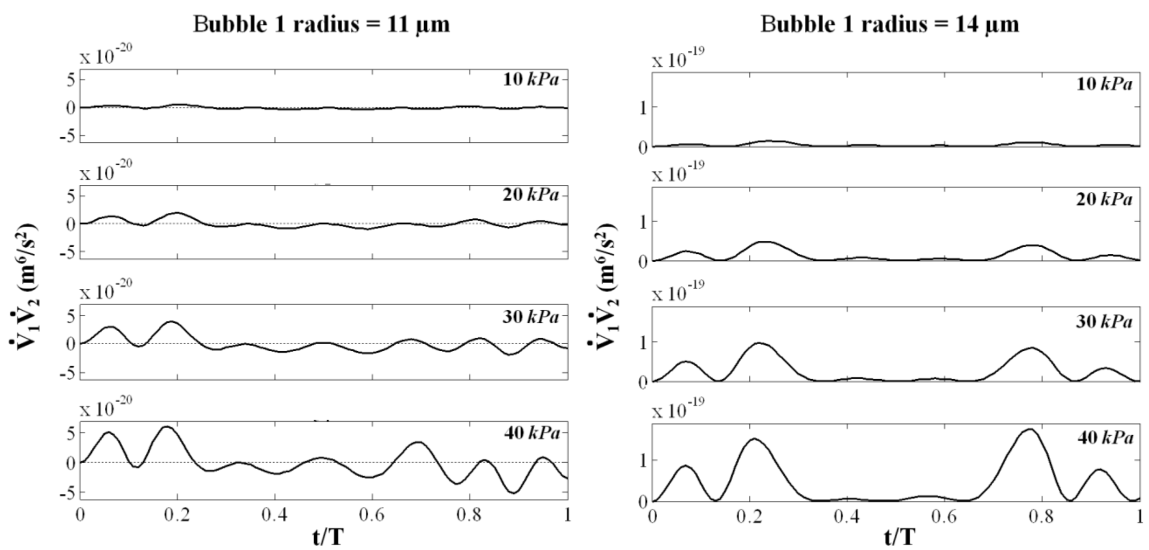

Bubble 1 radius = 11 μm
Bubble 1 radius = 14 μm
x 10^-20
x 10^-19
10 kPa
20 kPa
30 kPa
40 kPa
V̇1 V̇2 (m^6/s^2)
t/T

Figure 8

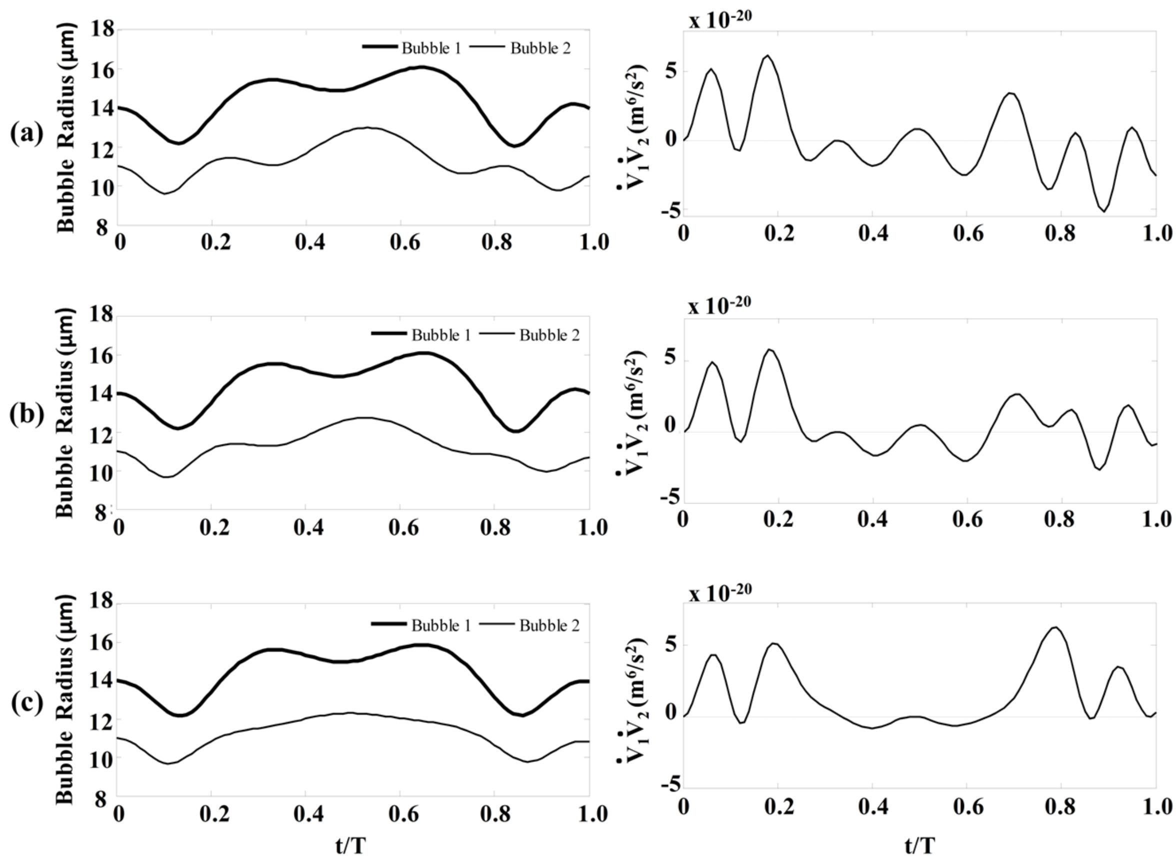
(a)
(b)
(c)
Bubble Radius (µm)
Bubble 1
Bubble 2
x 10^-20
$\dot{V}_1\dot{V}_2$ (m^6/s^2)
t/T